Pharmaceutical Sciences 2024: Navigating the Future of Drug Discovery and Development
November 2024

IN SILICO APPROACH TO DETERMINE TARGET SPECIFICITY OF SEVERAL PHYTOCONSTITUENTS AGAINST HUMAN ALPHA-DYSTROGLYCAN RECEPTOR: CHALLENGING LASSA VIRUS INFECTIVITY, VIRULENCE, AND PATHOGENICITY

Dr Uma Nath. U,
Professor
Department of Pharmaceutical Analysis
Sree Krishna College of Pharmacy and Research Centre,
Thiruvananthapuram, Kerala, India

ABSTRACT

For the discovery of agents from natural sources for effectively managing the numerous challenges (Infectivity, Virulence, and Pathogenicity) imposed by Lassa virus, the present study involved screening of few natural bioactives; (1) Peonidin; (2) β-Cryptoxanthin; 3) Zeaxanthin; (4) Hydroxy cinnamic acid; (5) Myricetin; (6) Quercetin; (7) Kaemferol; (8) Luteolin; (9) Apigenin; (10) Chlorogenic acid; (11) 3,4-di-*O*-caffeoylquinic acid; (12) 4,5-di-*O*-caffeoylquinic acid; (13) 3,4,5-tri-*O*-caffeoylquinic acid; (14) 1-Ipomeanol; (15) 4-Ipomeanol; (16) 1,4-Ipomeadiol; (17) Ipomeanine; (18) Cyanidin; (19) Delphinidin; and (20) Malvidin via *in silico* structure-based drug design (SBDD) technique by utilizing the Schrodinger Maestro 9.1 software against the crystal structure of human alpha-dystroglycan (PDB ID: 5LLK), a target known for the entrance of virus into host cells by interfering with the development of the glycoprotein. Also, drug-likeliness studies, bioavailability studies, and pharmacokinetic studies have been performed for the most effective compound, Malvidin using SwissADME online tool. The study will provide clues, motivate, and throw light on imperative aspects for the globally working medicinal chemists in the rational designing of anti-infective drugs in the near future.

Keywords: Lassa virus, α-dystroglycan, Molecular docking, Pharmacokinetics, Phytoconstituents, *In silico*

1. INTRODUCTION

Among the people that live in Western Africa, Lassa fever (LF) is endemic [1]. The rat *Mastomys natalensis* is the primary reservoir and transmitter of the *Lassa mammarenavirus* (LASV) that causes the sickness in mammals [2]. The most lethal arenavirus, Lassa virus, is a member of the Old World (OW) virus family [3]. In West Africa, LASV causes between 300,000 and 500,000 annual infections and 5,000 annual fatalities [4]. Biological fluids (urine, blood, saliva, feces) from infected hosts may transfer the LASV both zoonotically and between humans [5]. The primary symptoms of LF take from 3 days to 21 days to appear in human [6]. These include fever, nausea, and bleeding, as well as neurological, pulmonary, and gastrointestinal problems.

When it comes to gaining access to the host cell, the virion glycoprotein (GP) is where it is at for LASV. The SSP-GP1-GP2 trimer's GP1 binds to the host cell's α-dystroglycan (α-DG) receptor [7]. α-Dystroglycan is highly expressed in all human tissues and acts as a connection between the extracellular matrix and the cytoskeleton [8]. Post-translational glycosylation of α-DG by glycosyltransferase is required for normal biological activity and is also necessary for the recognition and binding of the LASV GP1 to α-DG [9]. Attachment of virion glycoproteins to extracellular α-DG triggers phosphorylation of α-DG at its tyrosine residues, paving the way for late endosomal transit of the viral particle [10]. After entering the cell, GP is processed to release a stable signal peptide (SSP) and an early GP1/GP2 complex. Cleavage of the GP1/GP2 complex into N-terminus GP1 and C-terminus GP2 subunit occurs after translocation to the Golgi apparatus [11]. The GP1 then undergoes a conformational change in a low acidic environment (pH 5), where it supports the receptor transition from α-DG to lysosome-associated membrane protein 1 (LAMP1), leading to viral genome membrane fusion, replication, transcription, and translation [7]. Thus, preventing LASV entrance into host cells by interfering with the development of the GP1 and α-DG receptor complex may disrupt the whole infection process.

Obtaining crystals of antigen-antibody complexes, determining their 3D structures via X-ray crystallography, etc. are just some of the time-consuming and money-consuming steps involved in experimentally identifying a random viral epitope [12]. Therefore, finding and using antiviral medications may be a more practical method than developing new vaccines. The antimicrobial, anti-inflammatory, and analgesic properties of naturally occurring chemical components originating from plants have all been extensively researched [13]. Many different phytochemicals have been shown to be effective against many viruses, including herpes simplex virus type 1 (HSV-1), human cytomegalovirus (HCV), poliovirus, avian influenza virus (IAV), dengue virus (DENV), and others. By interfering with the LASV replication cycle, tangeretin (pentamethoxyflavone) is able to halt the spread of Lassa virus [14]. Therefore, it is a potential technique to test naturally occurring chemicals for anti-infectious efficacy against LASV.

The main objective of this study was to explore the potential of 20 bioactive compounds [(1) Peonidin; (2) β-Cryptoxanthin; 3) Zeaxanthin; (4) Hydroxy cinnamic acid; (5) Myricetin; (6) Quercetin; (7) Kaemferol; (8) Luteolin; (9) Apigenin; (10) Chlorogenic acid; (11) 3,4-di-*O*-caffeoylquinic acid; (12) 4,5-di-*O*-caffeoylquinic acid; (13) 3,4,5-tri-*O*-caffeoylquinic acid; (14) 1-Ipomeanol; (15) 4-Ipomeanol; (16) 1,4-Ipomeadiol; (17) Ipomeanine; (18) Cyanidin; (19) Delphinidin; and (20) Malvidin] as anti-LASV agent by using Induced-Fit Molecular Docking approach. Also, drug-

likeliness studies, bioavailability studies, and pharmacokinetic studies have been performed for the most effective compound, Malvidin using SwissADME online tool.

2. MATERIALS AND METHODS

2.1.1. Preparation of Ligand

The structures were created using the Schrodinger Software suite 2021-2's 2D-sketcher module. For docking analysis, the Maestro environment version 12.8 was employed. The stereoisomers of these ligands were created using the LigPrep programme. Using the Epik ionizer, a maximum of four poses with correct protonation states were created for each ligand at a target pH of 7.0. The OPLS 2005 force field was utilized to construct tautomerized, desalted ligands while keeping the input files' requisite chiralities, resulting in an optimized low energy 3D ligand [15].

2.1.2. Preparation of Protein

The crystal structure of human alpha-dystroglycan (PDB ID: 5LLK) was selected as the prime targets to be studied and was obtained exclusively from the RCSB Protein Data Bank (PDB). The protein structures were created using Maestro 9.1's Protein Preparation Wizard. The pre-processed and inspected structures were taken when developing the biological target. To get the right shape, the disulfide bonds, bond ordering, and formal charges were assigned using the Protein Preparation Wizard module of the Schrodinger Maestro 9.1. Co-factors, metal ions, water molecules in crystal formations beyond a distance of 5A°, and the hetero group were all removed. The "impref utility" tool was used to optimize hydrogen atoms by keeping all heavy atoms in their original positions, while the "H-bond assignment" tool was used to optimize the hydrogen-bonding network. Molecular docking was used to define the receptor (x, y, z) grids (-30 × -20 × 15) for the protein structure, allowing a variety of ligand poses to bind at the anticipated active site. Grids were built and placed at the ligand's centroid in such a way that they covered the whole ligand in a cubic box of defined measurement with the following characteristics: 1.00 Van der Waals scale factor and 0.25 charge cut off. The docking was done in XP mode, and only the energy-minimized postures were scored, which was expressed as a Glide score. The best-docked posture with the lowest Glide score value for each ligand was considered after the highest-scoring ligands were docked [16].

2.1.3. Induced-Fit Molecular Docking

The structure-based drug design process is restarted after the target protein's structure is understood. The stiff receptor was docked with the low-energy ligands, and the fit into the active site was evaluated,

as well as the predicted binding mechanism. In receptor-based computational techniques, the ligand interacting with the macromolecule protein (receptor) was represented using a molecular docking methodology. With low energy levels, IFD predicted that the ligand would have a good contact with the target. The method facilitates in the finding of low-free-energy conformations as well as the complete removal of steric conflicts. With 0.7 Van der Waals scaling for the receptor and 0.5 Van der Waals scaling for the ligand, side chains were eliminated, and a 0.18 RMSD value cut off, the maximum number of poses for each ligand remained at 20. The chemicals were ranked based on the information obtained, and a selection was tested for biological activity experimentally. The Glide Score was determined for each ligand [17].

2.2. Pharmacokinetics, Bioavailability, and Drug-likeliness studies

The SwissADME online tool was used to conduct a prediction research of pharmacokinetics, namely ADME, bioavailability, and drug-likeness of ligands. To identify drug-likeness, the technology estimates bioavailability radar based on six physicochemical properties: lipophilicity, size, polarity, insolubility, flexibility, and insaturation. The ADME properties, such as passive human gastrointestinal absorption (HIA) and blood-brain barrier (BBB) permeation, as well as substrate or non-substrate of the permeability glycoprotein (P-gp) was detected positive or negative in the BOILED-Egg model within the tool. The lipophilicity estimation (Log p/w) parameters such as iLOGP on free energies of solvation in n-octanol and water calculated by the generalized-born and solvent accessible surface area (GB/SA) model, XLOGP3 is an atomistic method with corrective factors and a knowledge-based library, WLOGP is an implementation of a purely atomistic method, and MLOGP is an archetype of topological method rely The Lipinski (Pfizer) filter, which was the first rule-of-five to be implemented in a tool, was used to predict drug-likeness. The bioavailability radar was used to predict oral bioavailability based on several physicochemical characteristics. The ranges of each parameter was mentioned as LIPO = lipophilicity as -0.7 < XLOGP3 < +5.0; SIZE = size as molecular weight 150gm/mol < MV < 500gm/mol; POLAR = polarity as 20Å² < TPSA (topological polar surface area) < 130Å²; INSOLU = insoluble in water by log S scale 0 < Logs (ESOL) < 6; INSATU = insaturation or saturation as per fraction of carbons in the sp^3 hybridization 0.3 < Fraction Csp3 < 1 and FLEX = flexibility as per rotatable bonds 0 < Number of rotable bonds < 9 [18].

3. RESULTS AND DISCUSSION

3.1. Molecular docking

The most promising inhibitor was found to be Malvidin with Glide Score of –5.264 Kcal/mol by interacting with amino acid residues ARG76 [through –OH (hydroxyl), -O atom of OCH_3 as well as THR192 through –OH (hydroxyl)] along with π-cation interaction via amino acid residues LYS226 and LYS302 through aromatic component in the structure. The natural compound with lowest Glide Score (-2.195 Kcal/mol) was identified as 3,4,5-tri-*O*-caffeoylquinic acid. The interaction of several bioactive compounds against human α-dystroglycan is described in **Table 1**.

Table 1. Interaction of several bioactive compounds against human α-dystroglycan to challenge Lassa virus infectivity.

S. No.	Compounds	Binding Energy (Kcal/mol)	No. of H Bonds	Interacting residues	Van der Waals & other interactions
•	Peonidin	-5.122	2	THR192 (-OH), PHE236 (-OH)	LYS226, LYS302 (π-cation-aromatic)
•	Cryptoxanthin	-3.917	0	-	-
•	Zeaxanthin	-3.744	1	ASN267 (-OH)	-
•	Hydroxy cinnamic acid	-5.242	4	THR192 (-OH), ARG234 (=O), PHE236 (-OH), HIE298 (-OH)	-
•	Myricetin	-4.944	2	ARG76 (-OH), THR192 (-OH)	LYS226 (π-cation-aromatic)
•	Quercetin	-4.967	2	ARG76 (-OH), THR192 (-OH)	LYS226 (π-cation-aromatic)
•	Kaemferol	-4.271	0	-	LYS302 (π-cation-aromatic)
•	Luteolin	-4.785	1	THR192 (-OH)	LYS302 (π-cation-aromatic)
•	Apigenin	-4.444	0	-	LYS226 (π-cation-aromatic)
•	Chlorogenic acid	-4.261	3	THR192 (-OH), ASN224 (-OH), ASP237 (-OH),	-
•	3,4-di-*O*-caffeoylquinic acid	-4.148	4	GLU159 (-OH), ARG234 (=O), PHE236 (-OH), HIE298 (-OH)	LYS226 (π-cation-aromatic)

•	4,5-di-*O*-caffeoylquinic acid	-4.075	3	GLU159 (-OH), ARG234 (2× -OH)	ARG234 (π-cation-aromatic)
•	3,4,5-tri-*O*-caffeoylquinic acid	-2.195	5	ASP160 (-OH), SER162 (-OH), LYS226 (-OH), ARG234 (=O), ASP237 (-OH)	-
•	1-Ipomeanol	-4.212	1	ASP237 (-OH)	ARG234 (π-cation-aromatic)
•	4-Ipomeanol	-3.686	3	LYS226 (-OH), THR192 (-OH), ARG234 (-O of Furan)	HIE298 (π- π stacking-aromatic)
•	1,4-Ipomeadiol	-4.327	3	LYS226 (-OH), SER259 (-OH), ARG234 (-O of Furan)	HIE298 (π- π stacking-aromatic)
•	Ipomeanine	-3.918	1	ARG234 (-OH)	-
•	Cyanidin	-4.481	1	ARG234 (-OH)	LYS226, LYS302 (π-cation-aromatic)
•	Delphinidin	-4.032	4	THR192 (2× -OH), PRO229 (-OH)	LYS226 (π-cation-aromatic)
•	Malvidin	-5.264	3	ARG76 (-OH, -O of OCH_3) THR192 (-OH)	LYS226 (π-cation-aromatic)

1

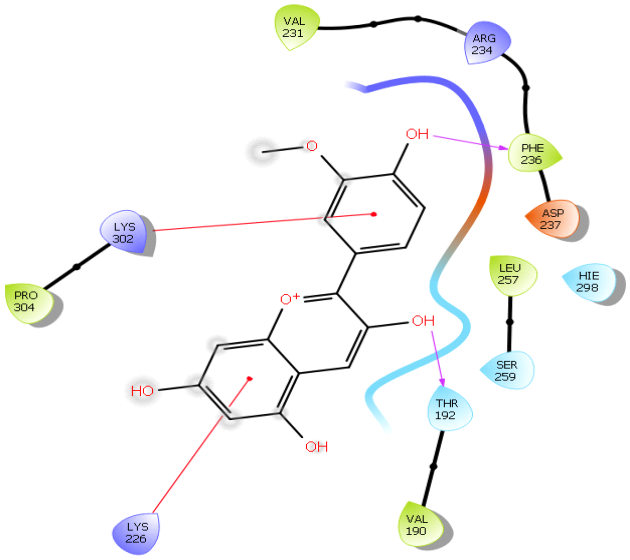

2

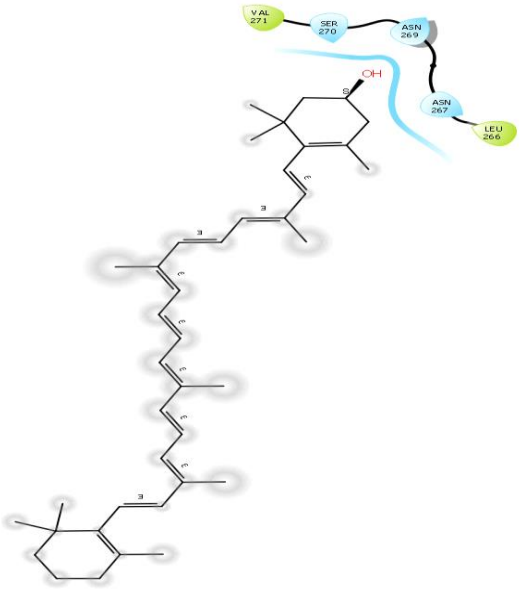
VAL 271
SER 270
ASN 269
OH
ASN 267
LEU 266

3

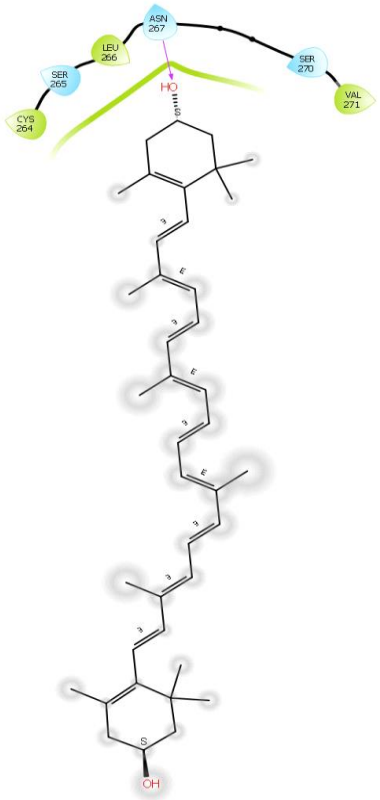
ASN 267
LEU 266
SER 265
CYS 264
HO
SER 270
VAL 271
OH

4

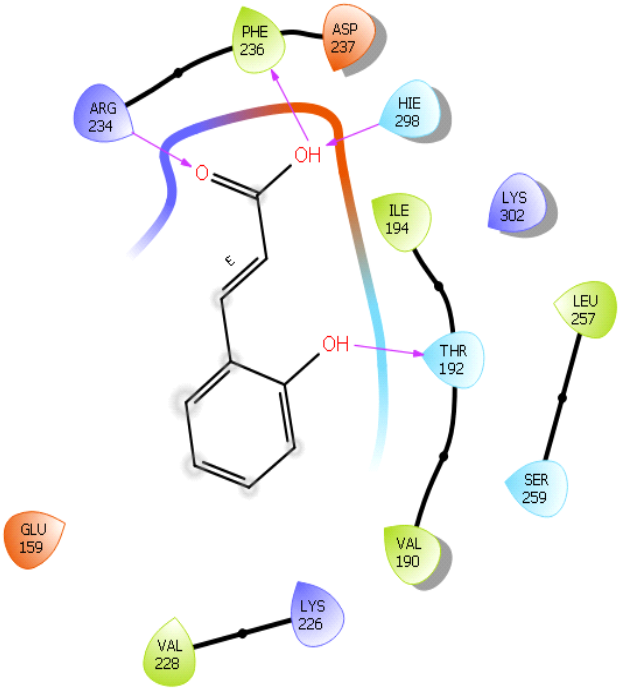
PHE 236
ASP 237
ARG 234
HIE 298
OH
O
LYS 302
ILE 194
LEU 257
OH
THR 192
SER 259
GLU 159
VAL 190
LYS 226
VAL 228

5

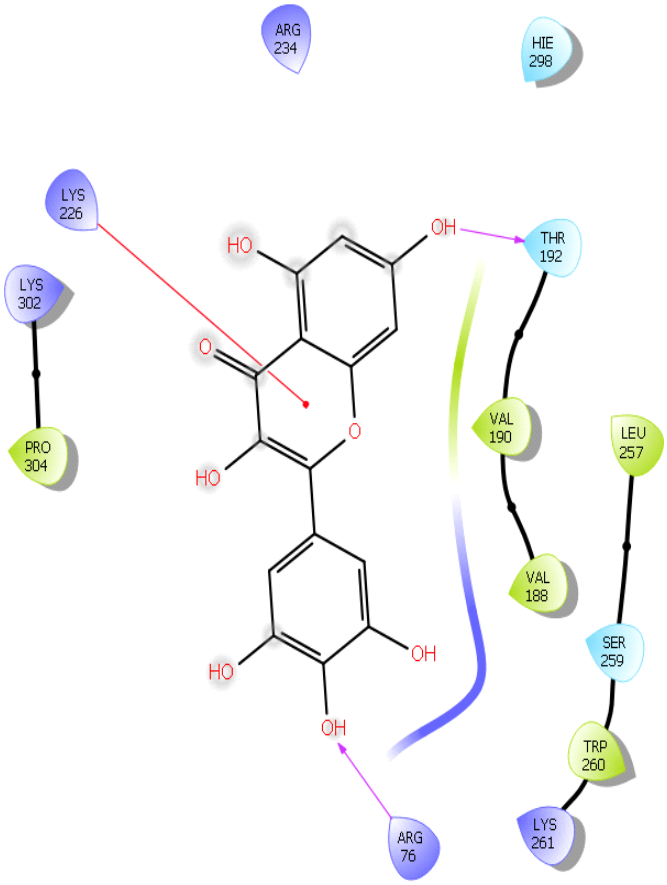
ARG 234
HIE 298
LYS 226
HO
OH
THR 192
LYS 302
O
O
PRO 304
HO
VAL 190
LEU 257
VAL 188
SER 259
HO
OH
OH
TRP 260
ARG 76
LYS 261

6

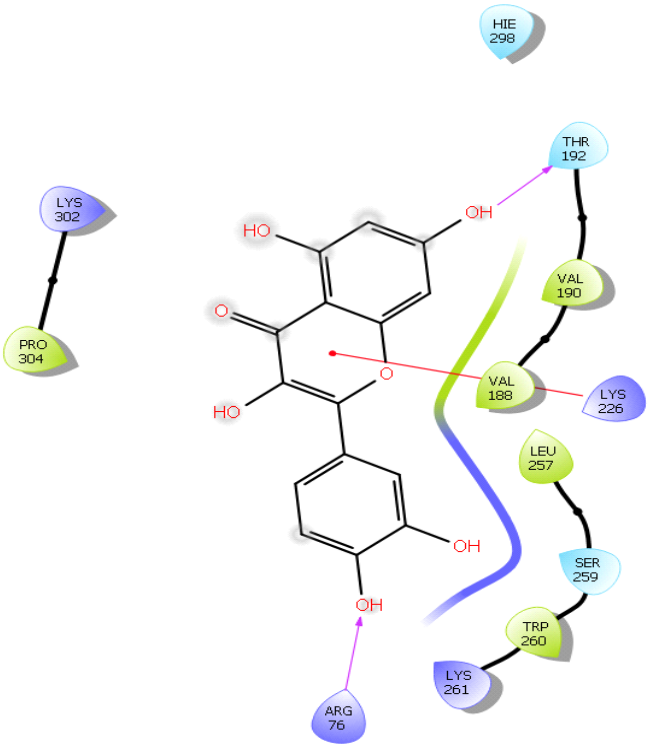
HIE 298
THR 192
LYS 302
OH
HO
VAL 190
O
PRO 304
O
VAL 188
LYS 226
HO
LEU 257
OH
SER 259
OH
TRP 260
LYS 261
ARG 76

7

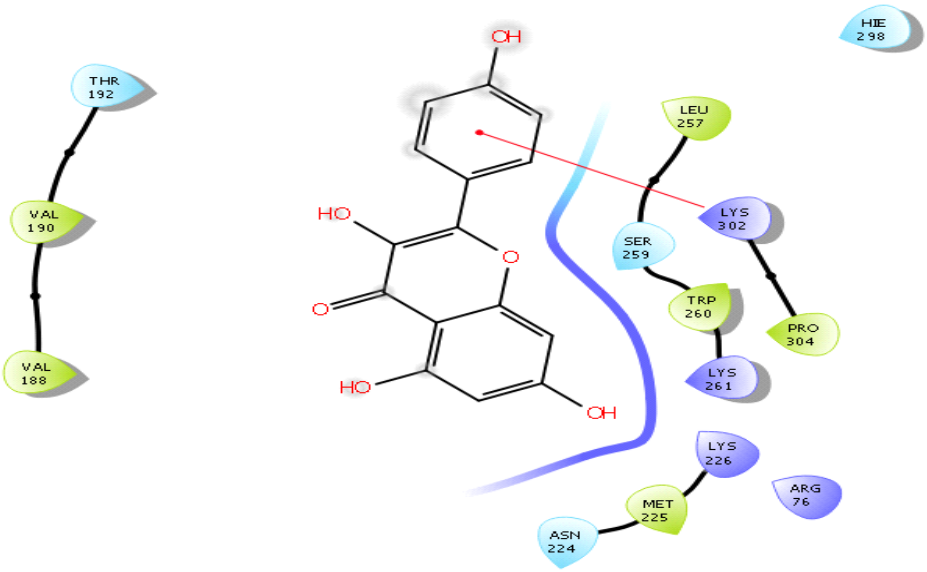
HIE 298
OH
THR 192
LEU 257
HO
LYS 302
VAL 190
O
SER 259
O
TRP 260
PRO 304
VAL 188
LYS 261
HO
OH
LYS 226
ARG 76
MET 225
ASN 224

8

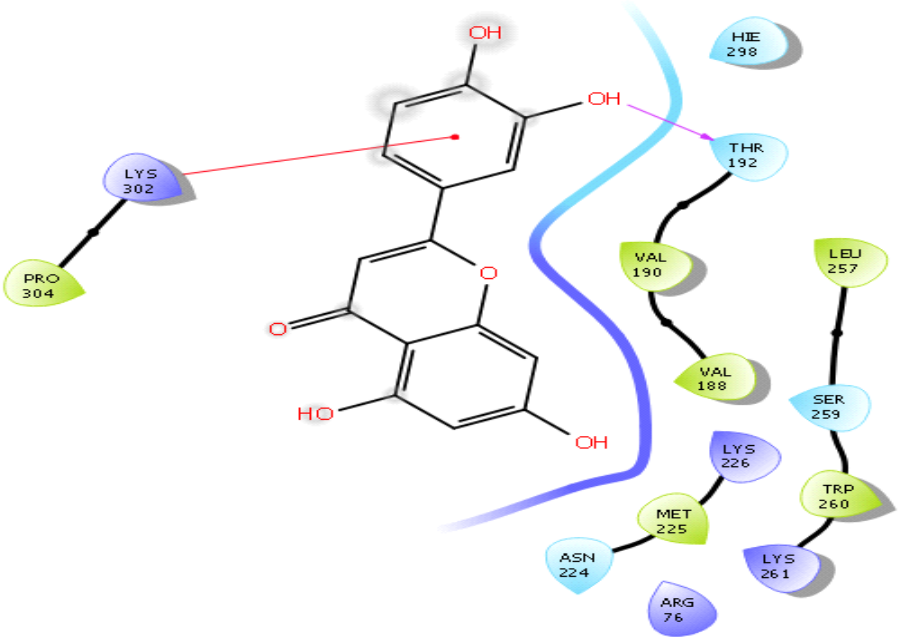
OH
OH
HIE 298
THR 192
LYS 302
PRO 304
VAL 190
LEU 257
VAL 188
SER 259
O
O
HO
OH
LYS 226
TRP 260
MET 225
ASN 224
LYS 261
ARG 76

9

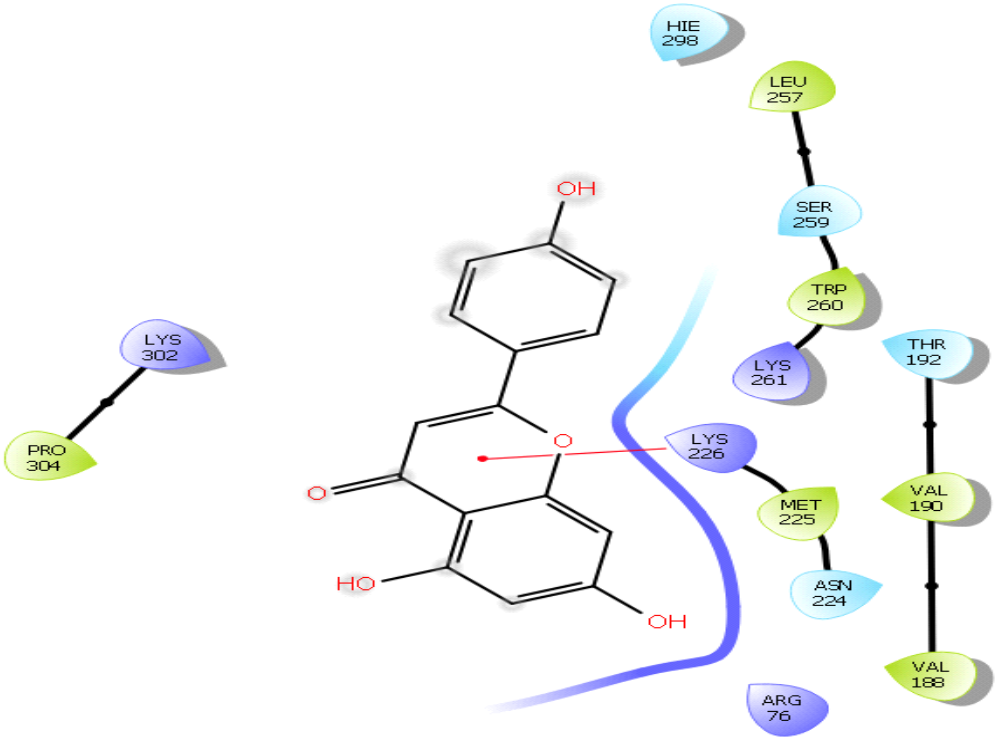
HIE 298
LEU 257
OH
SER 259
TRP 260
LYS 302
LYS 261
THR 192
O
LYS 226
PRO 304
MET 225
VAL 190
O
HO
ASN 224
OH
VAL 188
ARG 76

109

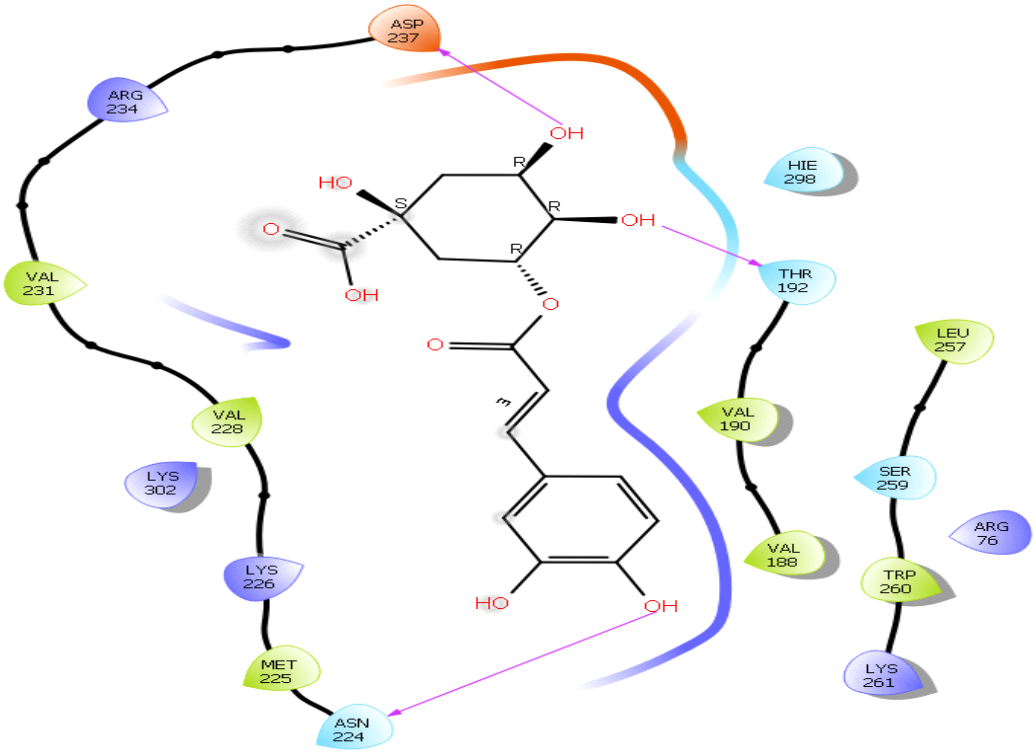
ASP 237
ARG 234
OH
HO
R
S
R
R
OH
O
OH
HIE 298
THR 192
VAL 231
O
O
3
LEU 257
VAL 190
VAL 228
SER 259
LYS 302
ARG 76
VAL 188
LYS 226
TRP 260
HO
OH
MET 225
LYS 261
ASN 224

119

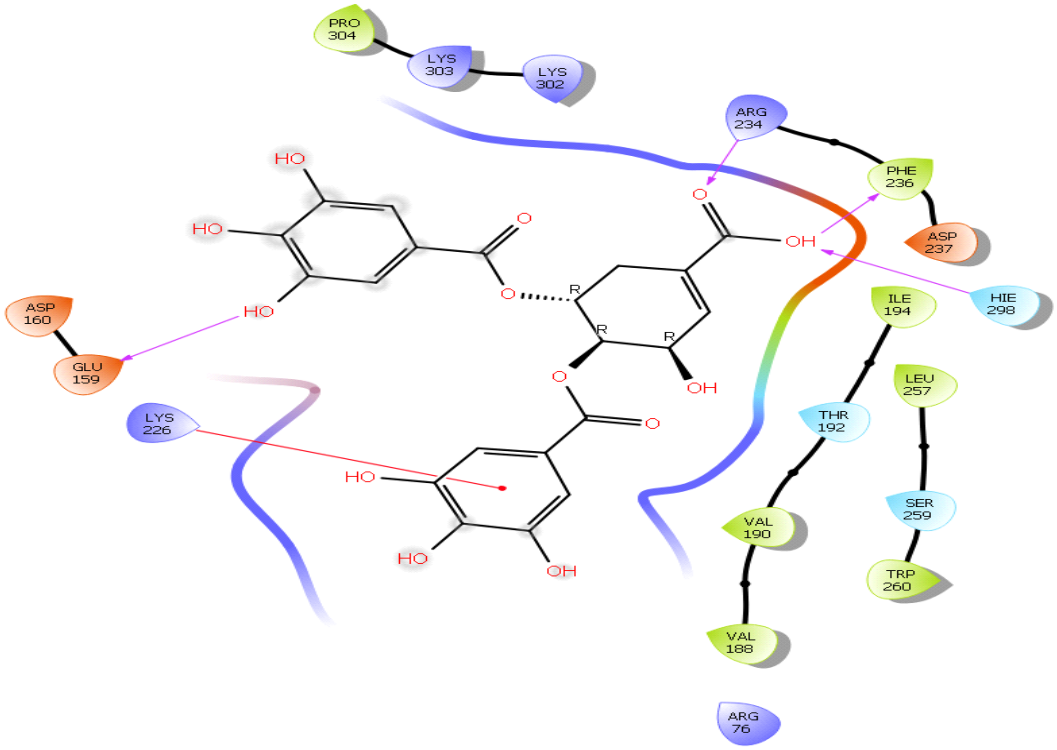
PRO 304
LYS 303
LYS 302
ARG 234
HO
PHE 236
HO
O
O
OH
ASP 237
O
R
HIE 298
ASP 160
HO
ILE 194
R
R
GLU 159
OH
LEU 257
O
THR 192
LYS 226
O
HO
SER 259
VAL 190
HO
OH
TRP 260
VAL 188
ARG 76

129

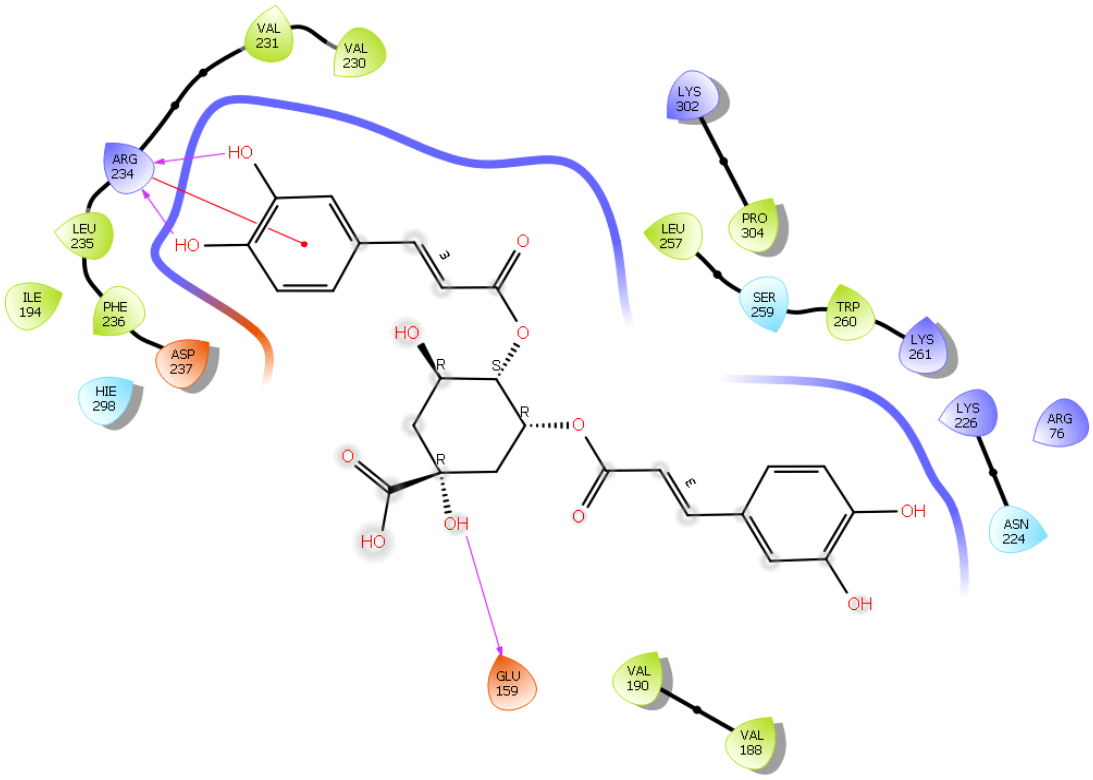
VAL 231
VAL 230
LYS 302
ARG 234
HO
HO
LEU 235
PRO 304
LEU 257
ILE 194
PHE 236
SER 259
TRP 260
LYS 261
ASP 237
HIE 298
HO
O
O
R
S
R
R
O
O
O
HO
OH
LYS 226
ARG 76
ASN 224
OH
OH
GLU 159
VAL 190
VAL 188

139

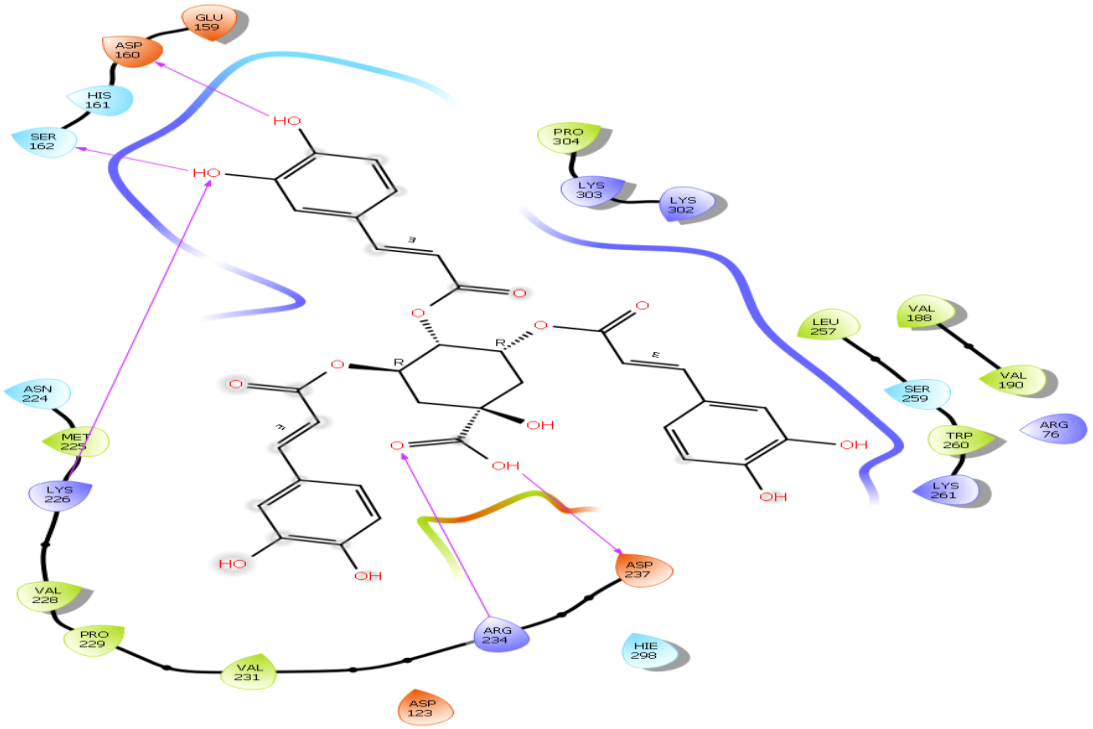
GLU 159
ASP 160
HIS 161
SER 162
HO
HO
PRO 304
LYS 303
LYS 302
LEU 257
VAL 188
VAL 190
SER 259
ASN 224
MET 225
LYS 226
TRP 260
ARG 76
LYS 261
OH
OH
OH
HO
OH
VAL 228
PRO 229
ARG 234
ASP 237
HIE 298
VAL 231
ASP 123

149

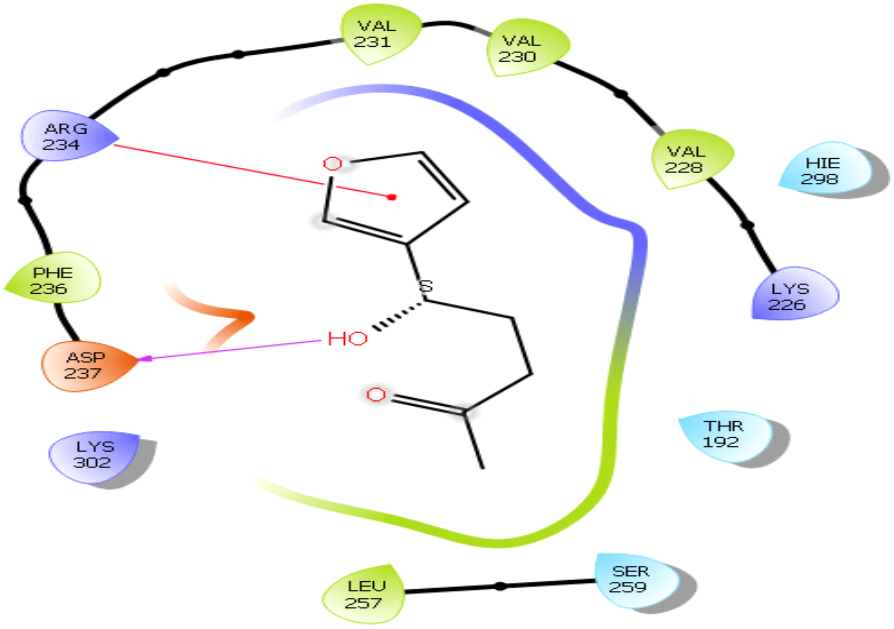
VAL 231
VAL 230
ARG 234
VAL 228
HIE 298
PHE 236
LYS 226
ASP 237
THR 192
LYS 302
LEU 257
SER 259

159

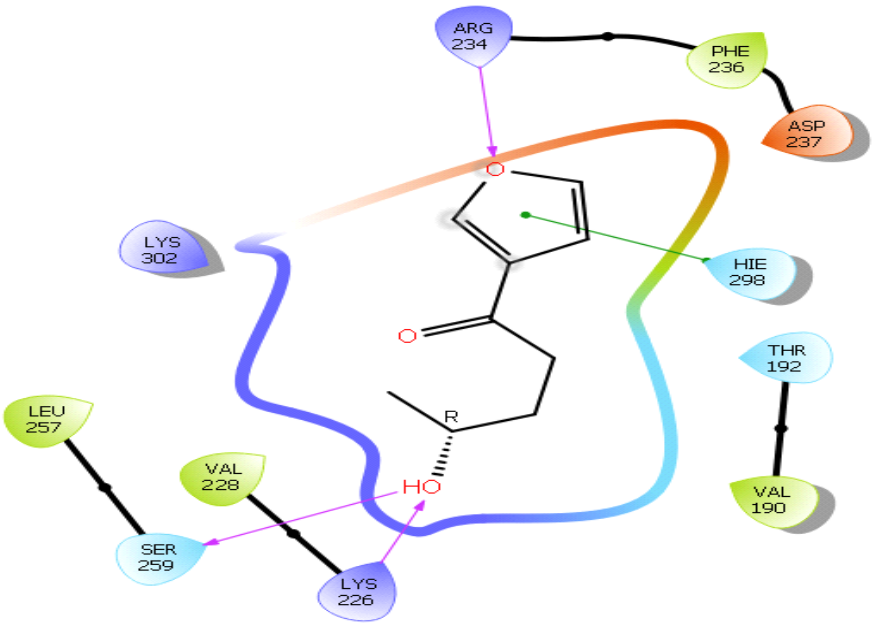
ARG 234
PHE 236
ASP 237
LYS 302
HIE 298
THR 192
LEU 257
VAL 228
VAL 190
SER 259
LYS 226

169

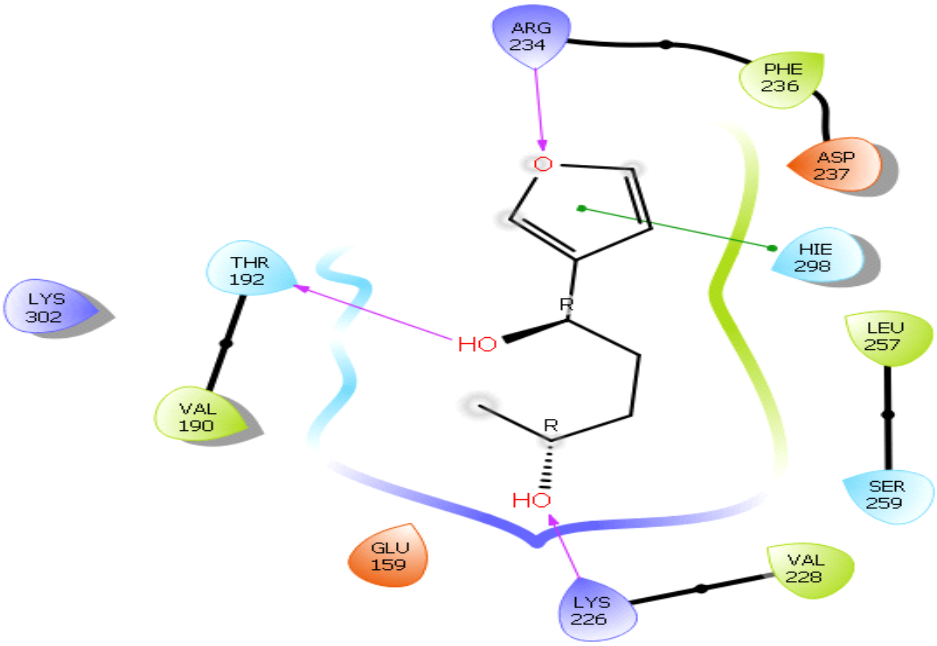
ARG 234
PHE 236
ASP 237
O
HIE 298
THR 192
LYS 302
R
HO
LEU 257
VAL 190
R
HO
SER 259
GLU 159
VAL 228
LYS 226

179

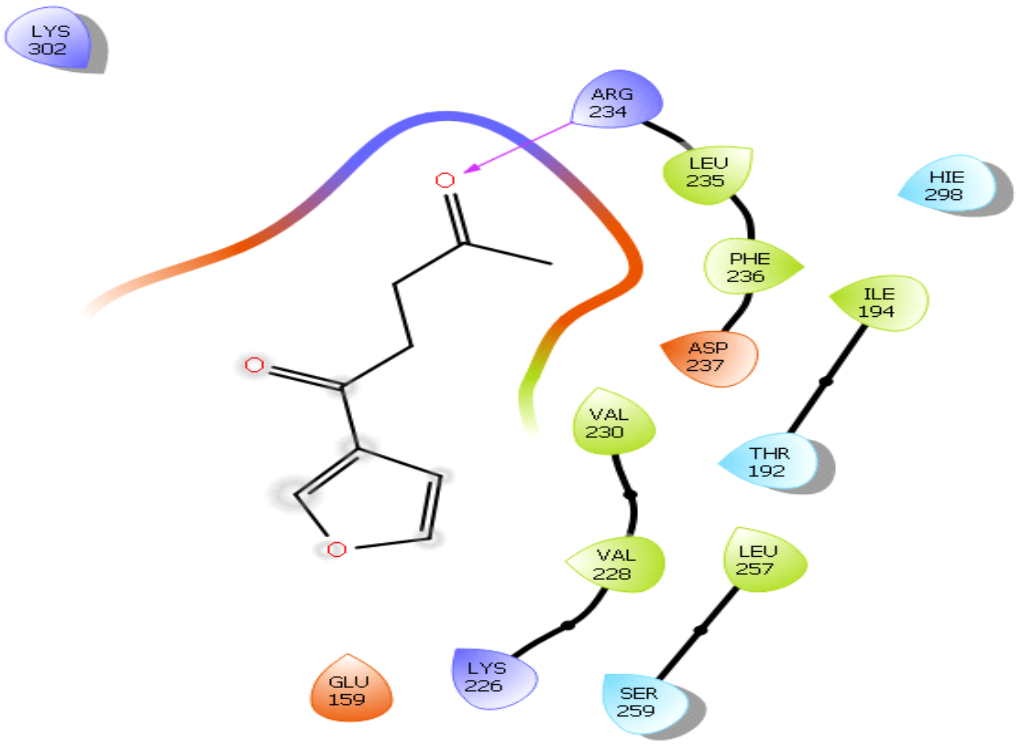
LYS 302
ARG 234
LEU 235
HIE 298
O
PHE 236
ILE 194
ASP 237
O
VAL 230
THR 192
O
VAL 228
LEU 257
GLU 159
LYS 226
SER 259

1809

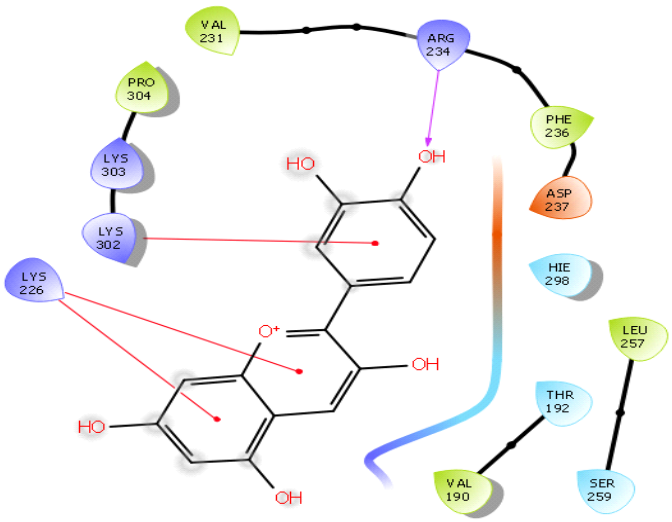
VAL 231
ARG 234
PRO 304
PHE 236
LYS 303
ASP 237
LYS 302
HIE 298
LYS 226
LEU 257
THR 192
VAL 190
SER 259
HO
OH
O+

199

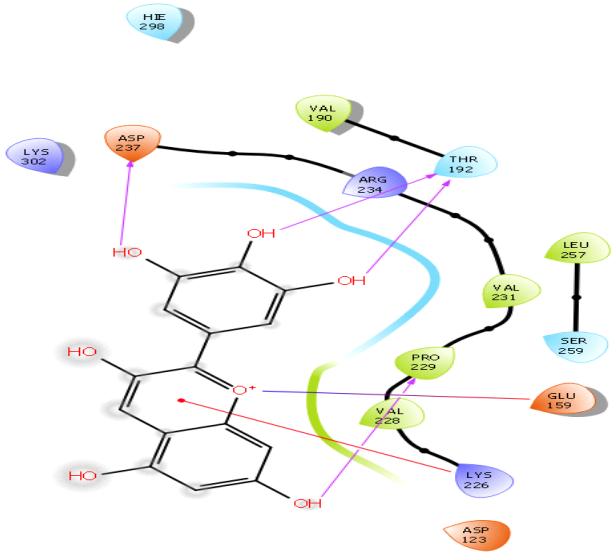
HIE 298
VAL 190
ASP 237
LYS 302
THR 192
ARG 234
LEU 257
VAL 231
SER 259
PRO 229
GLU 159
VAL 228
LYS 226
ASP 123
HO
OH
O+

209

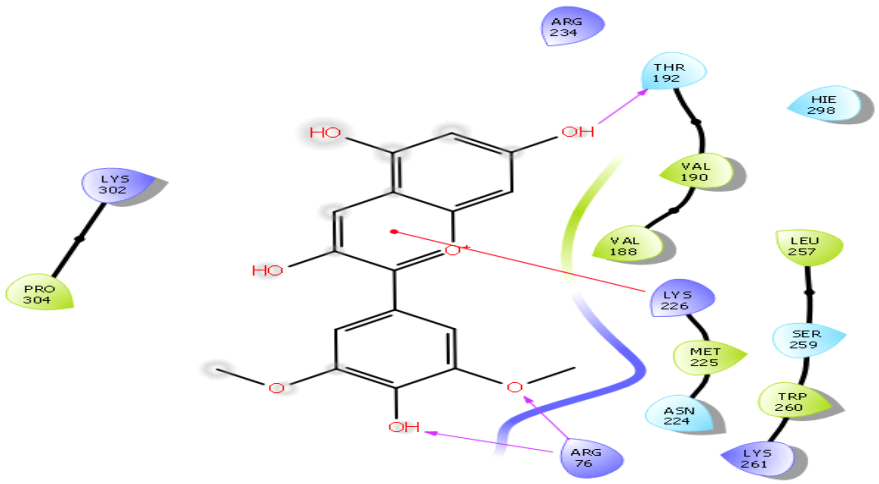

Figure 1. Docking poses of (1) Peonidin; (2) β-Cryptoxanthin; 3) Zeaxanthin; (4) Hydroxy cinnamic acid; (5) Myricetin; (6) Quercetin; (7) Kaemferol; (8) Luteolin; (9) Apigenin; (10) Chlorogenic acid; (11) 3,4-di-*O*-caffeoylquinic acid; (12) 4,5-di-*O*-caffeoylquinic acid; (13) 3,4,5-tri-*O*-caffeoylquinic acid; (14) 1-Ipomeanol; (15) 4-Ipomeanol; (16) 1,4-Ipomeadiol; (17) Ipomeanine; (18) Cyanidin; (19) Delphinidin; and (20) Malvidin against human α-dystroglycan.

2.2. Pharmacokinetics, Bioavailability, and Drug-likeliness studies

Table 2 describes the predictive values for pharmacokinetics, bioavailability and drug-likeness data on Malvidin. The molecule showed average oral absorption rate, high gastrointestinal absorption, no blood-brain permeability, and very lower skin permeation. In case of metabolism, the molecule was found to be a p-glycoprotein positive substrate, however, the molecule did not served as a substrate for CYP2C19, CYP2C9, CYP2D6 and CYP3A4. The drug-likeness study showed no violation of Lipinski's rule of 5 as well as other rules which indicated perfection in terms of physicochemical and pharmacological perspectives.

For the prediction of bioavailability, an average bioavailability score was obtained, although high water solubility was predicted for Malvidin. The bioavailability radar for oral bioavailability prediction showed desired INSATU = insaturation as per Csp3 as 0.12, FLEX as per number of rotable bond 3, INSOLU Logs (ESOL) as -3.60, SIZE as molecular weight (g/mol) of 331.30 (**Figure 2A**), POLAR as TPSA (Å²) 112.52, and LIPO as XLOGP3 value of 2.24 (**Figure 2B**).

In case of BOILED-Egg model (**Figure 2C**), it was obtained that Malvidin has low capability of blood-brain barrier penetration as well as it also showed low penetration power of gastrointestinal absorption. The molecule was neither PGP negative nor PGP positive as non-substrate in predictive model. Interestingly, the Brain Or IntestinaL EstimateD permeation method (BOILED-Egg) has

already been proposed as an accurate predictive model, which helps by computational prediction of the lipophilicity and polarity of small molecules. In overall predictive results, Malvidin can be suitable candidate as per bioavailability radar and BOILED-Egg representation. Furthermore, these predictive results should be validated by *in vitro* and *in vivo* functional and pharmacological assay for the management of various diseases originated through Lassa virus.

Table 2. Pharmacokinetics and physicochemical properties of Malvidin.

PROPERTIES	DATA
Physicochemical Properties	
Formula	$C_{17}H_{15}O_7$
Molecular weight	331.30 g/mol
Number of heavy atoms	24
Number of aromatic heavy atoms	16
Fraction Csp3	0.12
Number of rotatable bonds	3
Number of H-bond acceptors	7
Number of H-bond donors	4
Molar Refractivity	87.13
TPSA (A^2)	112.52
Lipophilicity	
Log Po/w (iLOGP)	-1.96
Log Po/w (XLOGP3)	2.24
Log Po/w (WLOGP)	3.22
Log Po/w (MLOGP)	0.28
Log Po/w (SILICOS-IT)	0.80
Consensus Log Po/w	0.92
Water Solubility	
Log S (ESOL)	-3.60
Solubility	8.31e-02 mg/ml ; 2.51e-04 mol/l
Class	Soluble
Log S (Ali)	-4.24
Solubility	1.91e-02 mg/ml ; 5.77e-05 mol/l
Class	Moderately soluble
Log S (SILICOS-IT)	-3.46
Solubility	1.14e-01 mg/ml ; 3.44e-04 mol/l
Class	Soluble
Pharmacokinetics	
GI absorption	High
BBB permeant	No
P-gp substrate	Yes
CYP1A2 inhibitor	Yes
CYP2C19 inhibitor	No
CYP2C9 inhibitor	No

CYP2D6 inhibitor	No
CYP3A4 inhibitor	No
Log Kp (skin permeation)	-6.73 cm/s
Drug-likeness	
Lipinski	Yes; 0 violation
Ghose	Yes
Veber	Yes
Egan	Yes
Muegge	Yes
Bioavailability Score	0.55
Medicinal Chemistry	
PAINS	0 alert
Brenk	1 alert; charged_oxygen_sulfur
Lead-likeness	Yes
Synthetic accessibility	3.33

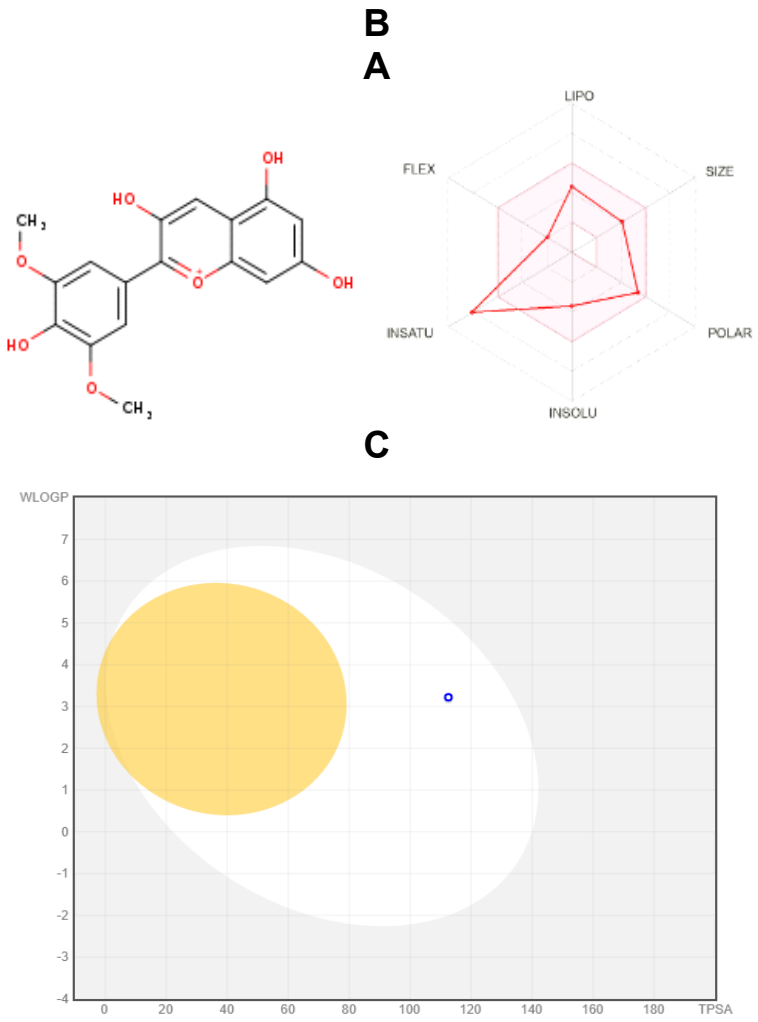

Figure 2. Pharmacokinetic predictions for Malvidin: (A) Chemical Structure, (B) Bioavailability radar plot, and (C) BOILED Egg Model.

4. CONCLUSION

The present study involved identification of novel bioactive compounds as potent anti-Lassa virus agents by inhibiting the target α-dystroglycan. It was clear from this research that all the compounds perfectly bound with the active site cavity of the biological target with varied levels. The most promising inhibitor was found to be Malvidin with Glide Score of –5.264 Kcal/mol whereas the natural compound with lowest Glide Score was identified as 3,4,5-tri-*O*-caffeoylquinic acid. The inhibitors demonstrated hydrogen bonding interactions directly as wells as through water molecules with the amino acid residues, and thus they could penetrate deeper into the active site cavity. These may provide the compounds a better orientation and can inhibit them complementary to the active site. Therefore, the research will undeniably motivate the modern day (medicinal) chemists and biologists to further explore and study the better halves of applications.

CONFLICT OF INTEREST

No conflict of interest is declared.

FUNDING INFORMATION

No agency provided any funds.

ACKNOWLEDGEMENT

The authors are highly thankful to the college management and colleagues for their continuous support.

5. REFERENCES

- Centers for Disease Control and Prevention. Lassa fever [EB/OL]. [2021-05-23]. https://www.cdc.gov/vhf/lassa/index.html.
- Garry RF. 50 years of Lassa fever research[J]. *Curr Top Microbiol Immunol,* 2020, doi: 10.1007/82_2020_214.
- Brisse ME, Ly H. Hemorrhagic fever-causing arenaviruses: lethal pathogens and potent immune suppressors[J]. *Front Immunol,* 2019, 10: 372.
- Olayemi A, Cadar D, Magassouba N, et al. New hosts of the Lassa virus[J]. *Sci Rep,* 2016, 6: 25280.
- Bonwitt J, Sáez AM, Lamin J, et al. At home with *Mastomys* and *Rattus*: human-rodent interactions and potential for primary transmission of Lassa virus in domestic spaces[J]. *Am J Trop Med Hyg,* 2017, 96(4): 935–943.
- Andersen KG, Shapiro BJ, Matranga CB, et al. Clinical sequencing uncovers origins and evolution of Lassa virus[J]. *Cell,* 2015, 162(4): 738–750.

- Torriani G, Galan-Navarro C, Kunz S. Lassa virus cell entry reveals new aspects of virus-host cell interaction[J]. *J Virol,* 2017, 91(4): e01902–16.
- Oppliger J, Torriani G, Herrador A, et al. Lassa virus cell entry *via* dystroglycan involves an unusual pathway of macropinocytosis[J]. *J Virol,* 2016, 90(14): 6412–6429.
- Fedeli C, Torriani G, Galan-Navarro C, et al. Axl can serve as entry factor for Lassa virus depending on the functional glycosylation of dystroglycan[J]. *J Virol,* 2017, 92(5):e01613–17.
- Moraz ML, Pythoud C, Turk R, et al. Cell entry of Lassa virus induces tyrosine phosphorylation of dystroglycan[J]. *Cell Microbiol,* 2013, 15(5): 689–700.
- Agnihothram SS, York J, Nunberg JH. Role of the stable signal peptide and cytoplasmic domain of G2 in regulating intracellular transport of the Junín virus envelope glycoprotein complex[J]. *J Virol,* 2006, 80(11): 5189–5198.
- Oscherwitz J. The promise and challenge of epitope-focused vaccines[J]. *Hum Vaccin Immunother,* 2016, 12(8): 2113–2116.
- Dey D, Paul PK, Azad SA, et al. Molecular optimization, docking, and dynamic simulation profiling of selective aromatic phytochemical ligands in blocking the SARS-CoV-2 S protein attachment to ACE2 receptor: an *in silico* approach of targeted drug designing[J]. *J Adv Vet Anim Res,* 2021, 8(1): 24–35.
- Tang K, He S, Zhang X, et al. Tangeretin, an extract from *Citrus* peels, blocks cellular entry of arenaviruses that cause viral hemorrhagic fever[J]. *Antiviral Res,* 2018, 160: 87–93.
- Singh RK, Mishra AK, Kumar P, Mahapatra DK. Molecular Docking and In Vivo Screening of Some Bioactive Phenoxyacetanilide Derivatives as Potent Non-Steroidal Anti-Inflammatory Drugs. *Int J Curr Rese Rev*, 2021; 13(10): S189-S196.
- Asati V, Bharti SK, Rathore A, Mahapatra DK. SWFB and GA strategies for variable selection in QSAR studies for validation of thiazolidine-2,4-dione derivatives as promising anticancer drug entities. Indian J Pharm Edu Res, 2017, 51(3): 436-451.
- Joseph TM, Sharanya CS, Mahapatra DK, Suresh KI, Sabu A, Haridas M. In vitro Assessment of Selected Benzoic Acid Derivatives as Anti-inflammatory Compounds. J Sci Indus Res, 2018, 77(6): 330-336.
- Chhajed SS, Chaskar S, Kshirsagar SK, Haldar AGM, Mahapatra DK. Rational design and synthesis of some PPAR-γ agonists: substituted benzylideneamino-benzylidene-thiazolidine-2,4-diones. Comp Biol Chem, 2017, 67: 260-265.